Antonio Laganà et al. (Eds.)

# Computational Science and Its Applications – ICCSA 2004

**International Conference
Assisi, Italy, May 2004
Proceedings, Part III**

**3** Part III

Springer

# Lecture Notes in Computer Science 3045

Antonio Laganà   Marina L. Gavrilova
Vipin Kumar   Youngsong Mun
C.J. Kenneth Tan   Osvaldo Gervasi (Eds.)

# Computational Science and Its Applications – ICCSA 2004

International Conference
Assisi, Italy, May 14-17, 2004
Proceedings, Part III

Springer

Volume Editors

Antonio Laganà
University of Perugia, Department of Chemistry
Via Elce di Sotto, 8, 06123 Perugia, Italy
E-mail: lag@unipg.it

Marina L. Gavrilova
University of Calgary, Department of Computer Science
2500 University Dr. N.W., Calgary, AB, T2N 1N4, Canada
E-mail: marina@cpsc.ucalgary.ca

Vipin Kumar
University of Minnesota, Department of Computer Science and Engineering
4-192 EE/CSci Building, 200 Union Street SE, Minneapolis, MN 55455, USA
E-mail: kumar@cs.umn.edu

Youngsong Mun
SoongSil University, School of Computing, Computer Communication Laboratory
1-1 Sang-do 5 Dong, Dong-jak Ku, Seoul 156-743, Korea
E-mail: mun@computing.soongsil.ac.kr

C.J. Kenneth Tan
Queen's University Belfast, Heuchera Technologies Ltd.
Lanyon North, University Road, Belfast, Northern Ireland, BT7 1NN, UK
E-mail: cjtan@optimanumerics.com

Osvaldo Gervasi
University of Perugia, Department of Mathematics and Computer Science
Via Vanvitelli, 1, 06123 Perugia, Italy
E-mail: ogervasi@computer.org

# Resonant Tunneling Heterostructure Devices – Dependencies on Thickness and Number of Quantum Wells

Nenad Radulovic, Morten Willatzen, and Roderick V.N. Melnik

Mads Clausen Institute for Product Innovation, University of Southern Denmark,
DK-6400 Sonderborg, Denmark
{radulle,willatzen,rmelnik}@mci.sdu.dk

**Abstract.** We present numerical results for GaAs/AlGaAs double-barrier resonant tunneling heterostructure devices. A particular emphasis is given to the influence of quantum well thickness and number of quantum well layers on current-voltage characteristic and carrier density profile. In the paper, we discuss results obtained for spatial dependencies of carrier densities, the peak and the valley current density, and corresponding potentials in N-shaped current-voltage characteristics for various resonant tunneling heterostructures. Results are based on the transient quantum drift-diffusion model. They are obtained by solving a coupled system of partial differential equations directly and, in contrast to previous analysis, no decoupling algorithms, procedures, or methods are used.

## 1  Introduction

Semiconductor devices that rely on quantum tunneling through potential barriers are playing an increasingly important role in advanced microelectronic applications, including multiple-state logic, memory devices, and high-frequency oscillators [1,2,3]. The local charge accumulation in quantum wells and nonlinear processes of charge transport across the barriers have been found to provide a number of mechanisms for Negative Differential Resistance/Conductance (NDR/C), bistability of the current at a given voltage, and nonlinear dynamics [4]. The N-shape of Current-Voltage Characteristics (IVC) may be adopted for realizing various logic functions.

By controlled layer-by-layer epitaxial growth of heterostructures in combination with lateral patterning, intricate artificial nanostructures with arbitrary shapes of barriers and wells can be designed and fabricated. Such bandstructure engineering can produce novel semiconductor devices with desired transport and optical properties. The aim of the current research activity in the field is not only to understand the complex and sometimes chaotic spatio-temporal dynamics of charge carriers in such structures, but also to make efficient use of those nonlinear transport properties in specific switching and oscillating electronic devices [4].

Physical device models are based on the physics of carrier transport, and can provide a great insight into the detailed operation of the device. In what follows, particular emphasis is placed upon low-dimensional GaAs/AlGaAs structures and the

nonlinear feedback between the space charges and the transport processes inherent in such structures. In Sect. 2, we present the physical model, as well as time and space discretization. Geometry and relevant parameters of the devices are mainly given in Sect. 3. A short description of numerical simulation is given in Sect. 4. Obtained results are presented and discussed in Sect. 5.

## 2   Theory and the Model

### 2.1   Origin and Validity of the Model

In the present paper, we employ the Transient Quantum Drift-Diffusion Model (TQDDM). It is a first-moment version of the isothermal Transient Quantum Hydrodynamic Model (TQHDM), where the velocity convection term is neglected [5]. The origin of the model is due to Ancona *et al.* [5,6]. The equation of state for the electron gas is generalized and density-gradient dependencies are included, which allow to account for quantum effects [5,6].

The TQDDM is limited to "high" temperatures ($T_0 \geq 77$ K) and "low" electron densities ($n \leq 3 \cdot 10^{19}$ electrons/cm$^3$), conditions often satisfied in semiconductor structure applications of most interest [7]. The density-gradient expansion is only valid if the coefficient ε, related to the quantum-correction term, is very small, ε << 1 [7]. Thus, the lowest-order density-gradient theory gives the best results when the characteristic length is large ($L > 10$ nm), and the effective mass close to its free-electron value [7].

### 2.2   The Transient Quantum Drift-Diffusion Model

A detailed derivation of the TQDDM is given by Pinnau *et al.* [8,9]. Basically, diffusion scaling is introduced in the TQHDM and the TQDDM is derived from a zero relaxation time limit.

The scaled TQDDM equations in 1D, stated on a bounded domain $\Omega \in R$, read [9]

$$n_t = \left( n F_x \right)_x \ , \tag{1a}$$

$$-\varepsilon^2 \frac{1}{\sqrt{n}} \left( \sqrt{n} \right)_{xx} + \log(n) + V = F \ , \tag{1b}$$

$$-\lambda^2 V_{xx} = n - C \ , \tag{1c}$$

where the dependent variables are: the electron density $n$, the quantum quasi-Fermi level $F$, and the electrostatic potential $V$. The time-independent doping profile $C$ represents the distribution of charged background ions. The scaled Planck constant ε, the scaled Debye length λ, and the scaled relaxation time $\tau_0$ (used in the numerical time discretization) are defined as

$$\varepsilon^2 = \frac{\hbar^2}{6m_e^* k_B T_0 L^2} \;\;,\;\; \lambda^2 = \frac{\varepsilon_s k_B T_0}{q^2 C_m L^2} \;\;,\;\; \tau_0^2 = \frac{k_B T_0 \tau^2}{m_e^* L^2} \;\;,$$

where physical constants are: the reduced Planck constant $\hbar$, the Boltzmann constant $k_B$, and the elementary charge $q$. Physical parameters are: the effective electron mass $m_e^*$, the device operating temperature $T_0$, the permittivity $\varepsilon_s$, and the relaxation time $\tau$, which depend on the material and the operating conditions of the device. The maximum absolute value of the doping profile $C$ is denoted as $C_m$, and $L$ is the characteristic (device) length.

The first term on the LHS of eq. (1b) is so-called quantum Bohm potential. The scaled current density, according to eq. (1a), is given by the following expression:

$$J = -nF_x \;\;. \tag{2}$$

Now, it is possible to introduce an external potential, modeling discontinuities in the conduction band, which occur in the resonant tunneling structures, and other semiconductor heterostructure devices [10]. For that reason, one must replace, in (1b), the potential $V$ by $V + B$ [10], where $B$ is a step function representing the nonnegative quantum well potential. The maximum value $B_m$, of the step-function $B$, depends on the content of Al in the ternary alloy composition. It is assumed that $B_m = 0.4$ eV, which corresponds to 65% Al in AlGaAs at 300 K [2].

In order to get a well-posed problem, the system of eqs. (1) has to be supplemented with appropriate boundary and initial conditions.

The electron density is assumed to fulfill local charge neutrality at the Ohmic contacts. Further, it is natural to assume that there is no normal component of the total current (including the quantum current) along the insulating part of the boundary. Finally, we require that no quantum effects occur at the contacts. These boundary conditions are physically motivated and commonly employed in quantum semiconductor modeling [10]. The numerical investigations in [11] underline the reasonability of this choice.

The boundaries are assumed to be at grid points 0 and $M$ (where $M + 1$ is the total number of grid points), e.g., at positions $x = 0$ and $x = L$, or in scaled coordinates, $x = 0$ and $x = 1$, respectively. The corresponding boundary conditions are given below:

$$\rho_{k,0} = \sqrt{C_0} \;\;,\;\; F_{k,0} = 0 \;\;,\;\; V_{k,0} = 0 \;\;, \tag{3}$$

$$\rho_{k,M} = \sqrt{C_M} \;\;,\;\; F_{k,M} = U \;\;,\;\; V_{k,M} = U \;\;, \tag{4}$$

where a new variable $\rho = \sqrt{n}$ has been introduced, and $U$ is an applied voltage.

The initial conditions for $\rho$, $F$ and $V$ are required to start numerical simulation in equilibrium case ($U = 0$ V). It is natural to set the initial values for $F$ and $V$ to zero, while one has the full freedom to choose/guess the initial value for $\rho$.

## 2.3 Discretization in Time and Space

One of the main requirements for the time-discretization is that the scheme should be stable [12,13]. Further, there is no need for higher-order schemes, since the overall discretization error will be dominated by the one introduced through the space-discretization [14,15]. Thus, schemes with first-order accuracy in the time step are sufficient. Moreover, in most of the numerical simulations for the classical Drift-Diffusion Model (DDM), schemes based on backward time differences are employed [12,14]. Since the TQDDM is an $O(\xi^2)$ correction of DDM, it is reasonable to assume this to be true [9]. The most prominent scheme fulfilling the above requirements is the implicit backward Euler method [14,15]. Afterwards, a convenient realizable discrete scheme is derived in two steps: a uniform spatial grid ($\Delta x = L/M$) is introduced, and the finite difference method is used [13,14,15].

# 3   Geometry and Relevant Parameters

A Quantum Well (QW) is a synthetic heterostructure containing a very thin layer (thickness of a few nanometers) of one semiconductor sandwiched between two (thin) layers of another semiconductor with a larger bandgap [3]. A superlattice is another important nanostructure, which arises if several alternating layers of two materials with different bandgaps are grown one by one. The potential profile of quantum wells and barriers, which show periodicity, is intimately connected with the charge transport properties of the nanostructures [4].

   In the present paper, the basic Double Barrier Resonant Tunneling Diode (DBRTD) consists of a quantum well GaAs layer sandwiched between two AlGaAs layers, each 5 nm thick. This resonant structure is itself sandwiched between two spacer GaAs layers of 5 nm thicknesses and supplemented with two contact GaAs regions, each 25 nm thick. The basic $n^+$-$n$-$n^+$ DBRTD in 2D is shown in Fig. 1. A superlattice has a similar structure with more than one barrier-QW-barrier alternating layers sandwiched between the space layers and supported with two contact regions.

   The contact regions are highly doped ($n^+$ type) with $C_m = 10^{24}$ m$^{-3}$, while the channel is moderately doped ($n$ type) with $C_m = 10^{21}$ m$^{-3}$. The distribution of charged background ions is described by the doping profile $C$, which is time independent. Such a device exhibits NDR/C due to electron tunneling through the potential barriers. A typical stationary N-shape IVC is well known from the literature.

   The domain in 1D case is the interval $\Omega = [0,L]$, $L > 0$ being the device length. The device length is a sum of all layers/regions of the heterostructure. The relaxation time is fixed at $\tau = 10^{-12}$ s [10]. It is assumed that the devices are operating at liquid-nitrogen temperature, $T_0 = 77$ K. The effective electron mass is chosen to be $m_e^* = 0.067 \cdot m_0$, where $m_0$ is electron rest mass. The permittivity of GaAs/AlGaAs is chosen as $\varepsilon_s = 13.1 \cdot \varepsilon_0$, where $\varepsilon_0$ is permittivity in vacuum. It is also assumed that we operate close to the thermal equilibrium.

GaAs 25 nm (n+)    GaAs 5 nm (n)    AlGaAs 5 nm (n)    GaAs 5 nm (n)    AlGaAs 5 nm (n)    GaAs 5 nm (n)    GaAs 25 nm (n+)

Ohmic contact    Ohmic contact

Contact Region    Spacer Layer    Barrier    Quantum Well    Barrier    Spacer Layer    Contact Region
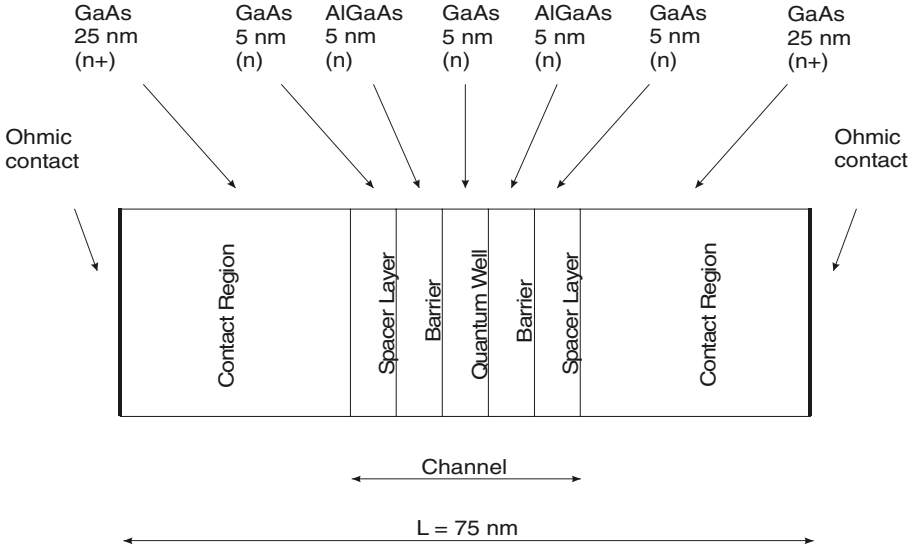
Channel

L = 75 nm

**Fig. 1.** Basic double barrier resonant tunneling semiconductor structure

## 4   Numerical Simulation

The numerical simulation is implemented in the Matlab. The system of discretized equations is solved in fully coupled manner for the first time, i.e., in the present work no decoupling algorithms, procedures, or methods are used.

To solve the nonlinear discrete system of equations, which follows from (1), the Newton Iteration Procedure (NIP) is employed [16], where the previous time step is used as initial guess. The following termination criterion is used to stop NIP:

$$\max_{k,l}\left(\left|u_{k,l}^{new} - u_{k,l}^{old}\right|\right) \le \tau_0 10^{-6} , \tag{5}$$

where $u$ denotes one of the variables $\rho$, $F$ and $V$. The indexes $k$ and $l$ correspond to the time and the space discretization, respectively. Convergence is assumed when the residuals are smaller than a set tolerance.

The scaled time step is changed during the time evolution. Initially, it is set to $10^{-6}$ and afterwards increased. The algorithm for the time step is based on two criterions: to speed up the time evolution and to ensure the convergence. The maximum number of required steps in the NIP is less than or equal to 5. Stationary solutions are reached after approximately 150 time steps, depending upon the semiconductor heterostructure under consideration. As a test example for the steady state, the total time is fixed to $T = 100\tau$ and the same results are obtained.

A uniform grid is used for space discretization. The resolution is set to 4 ppnm (points per nm). It gives us $M = 300$ for the basic case of a 75 nm DBRTD. We have checked the convergence of calculated variables ($\rho$, $F$, and $V$) by increasing the resolution (decreasing the grid size) and obtained a relative error less than 1% when 4 ppnm is used.

The obtained results for electron density $n$, quantum quasi-Fermi level $F$, and electrostatic potential $V$ are smooth and good agreement in the case of a basic DBRTD heterostructure, also considered in [10], is obtained. Excellent symmetry for equilibrium state ($U = 0$ V) is present for all semiconductor heterostructures under consideration. The current density in steady state has almost the same value at the Ohmic contacts, as required (relative error is less than 0.5%).

## 5   Results

Here, we present results for different resonant tunneling heterostructures, obtained with the numerical simulation. In the first case, a DBRTD with one QW is considered corresponding to three different QW sizes (2, 5, and 10 nm), while in the second case, superlattices with 2, 3, and 5 QWs are considered, where each QW is of the same size (5 nm). In all presented cases, width of the barriers and space layers are 5 nm. The length of all DBRTDs is fixed to $L = 75$ nm (contact regions are 26.5, 25, and 22.5 nm, respectively), while the length of the superlattices is a sum of all layers (contact regions are fixed to 25 nm). The external potential $U$ is always applied on the RHS Ohmic contact, while the LHS contact is grounded. In what follows, we are interested in the spatial dependency of electron densities and afterwards we comment on obtained current-voltage (IV) characteristics.

The results for electron densities for all three DBRTD (QW width 2, 5, and 10 nm), are given in Fig. 2. As a reference, doping profiles are also given. The applied potential is $U = 0.2$ V, which approximately corresponds to the peak voltage for these three cases. The results are qualitatively different for various thicknesses of the QW. For the case of a 2 nm QW, accumulation of electrons in the QW is evident, however, the resulting density for the "peak"-applied voltage is much less than the doping concentration. For the cases of 5 and 10 nm QW, the accumulation effect of electrons in the QW is indeed very important, and electron densities, for the peak-applied voltage, are significantly larger than doping concentration (two orders of magnitude). This indicates that a minimum thickness of the QW exists, which allows sufficient accumulation of electrons. In addition, the electron density inside the QW shows an increase of spatial asymmetry as the thickness of the QW is increased. A significant electron density reduction is apparent in the barrier regions and the minimums are not the same on both sides of the QW. The densities inside barriers have larger values on the side where the external potential is applied, in contrast to the densities inside the QW. The minimum of the density in the barrier changes significantly with increasing thickness of the QW. In contrast, the peak of the electron density inside QWs of different thicknesses shows "saturation", i.e., they are almost the same (if the thickness of the QW is large enough, $L_{QW} \geq$ 4-5 nm).

The results for electron densities for the superlattice heterostructures (with 2, 3, and 5 QWs), are given in Fig. 3. As a reference, doping profiles are also given. The applied potentials are $U = 0.30$ V, 0.35 V, and 0.50 V, which approximately correspond to the peak voltages, respectively. The superlattice heterostructures have different peaks of electron density in different QWs, under the influence of an external potential. In the case of a superlattice with 2 QWs, the charge accumulation in the QW being closer to the side where the external potential is applied, is much smaller, as is the peak. In the case of a superlattice with more than 2 QWs, the peak of
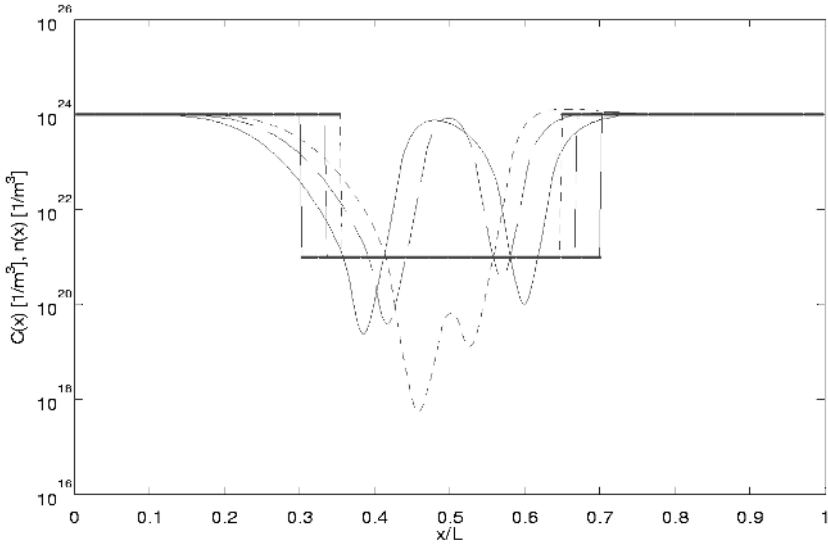
**Fig. 2.** Densities of electrons $n(x)$ for the DBRTDs with 2, 5, and 10 nm QW; dotted, dashed, and solid curve, respectively; $U = 0.2$ V; corresponding doping profiles $C(x)$ are represented by bold step-curves with the same line coding as for $n(x)$
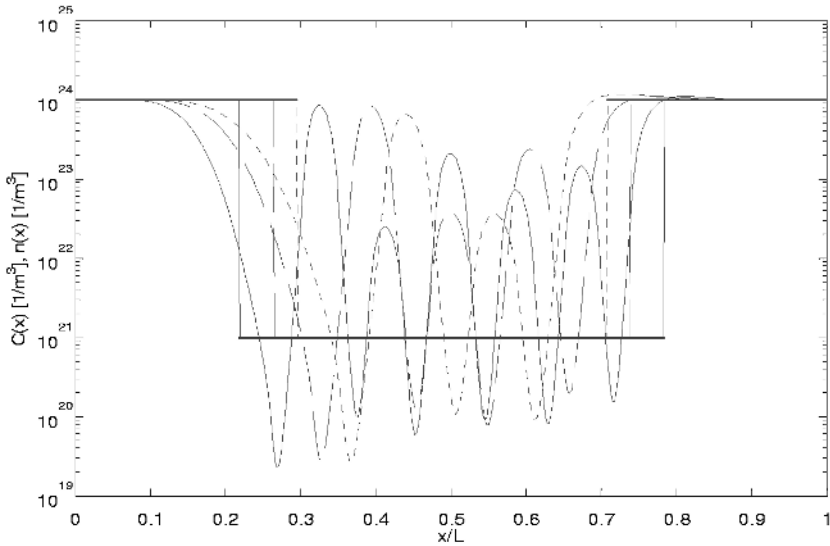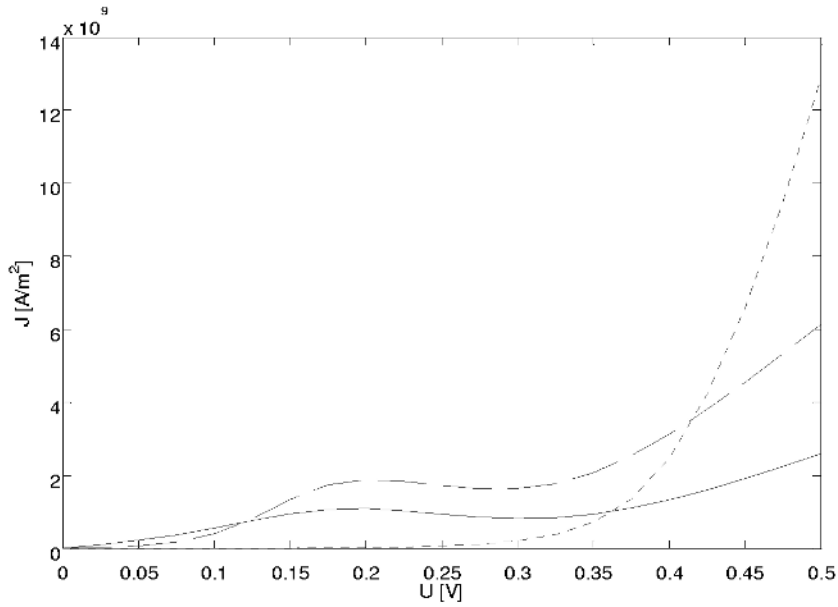


**Fig. 3.** Densities of electrons $n(x)$ for the superlattices with 2, 3, and 5 QWs; dotted, dashed, and solid curve, respectively; $U = 0.30$ V, $0.35$ V, and $0.50$ V, respectively; corresponding doping profiles $C(x)$ are represented by bold step-curves with the same line coding as for $n(x)$

**Fig. 4.** The IV characteristics for the DBRTDs with 2, 5, and 10 nm QW; dotted, dashed, and solid curve, respectively
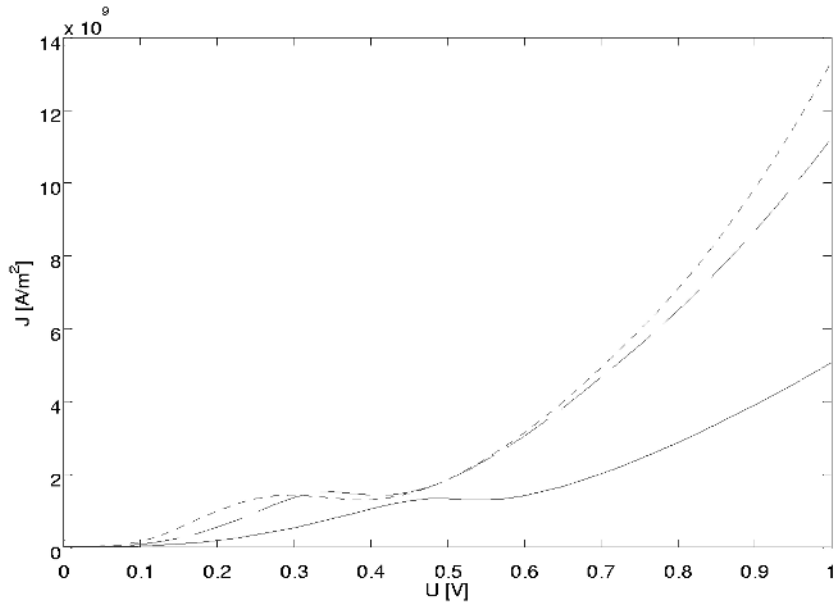


**Fig. 5.** The IV characteristics for the superlattices with 2, 3, and 5 QWs; dotted, dashed, and solid curve, respectively

the electron density inside QWs changes its magnitude, from the side where the external potential is applied towards the zero-volt (grounded) contact. In general, the QW that is closest to the zero-volt contact has the largest peak of the electron density. In contrast, the minimum of the electron density is always reached in the barrier that is nearby the zero-volt contact.

The IV characteristics for the DBRTDs (QW thickness of 2, 5, and 10 nm), are given in Fig. 4. The IV characteristic for the DBRTD with 2 nm QW does not show NDR/C at all. Changing the width of the QW, a significant change in the IV characteristic occurs, i.e., the current density for the same applied voltage is changed. In addition, the peak and the valley current density, and the relative ratio between them, also change significantly. However, the peak and the valley potential will only slightly differ.

The IV characteristics for the superlattice heterostructures with 2, 3, and 5 QWs (corresponding to $L = 85, 95, 115$ nm, respectively), are given in Fig. 5. It is obvious that an increase of the number of QWs leads to a significant influence on the IV characteristic. At the same time, the peak and the valley potential are also changed, and the current density is reduced. However, the peak and the valley current density will be only slightly changed.

Unfortunately, it is extremely difficult to predict the exact values of the peak and the valley current density in the N-shaped IV characteristics. These values are strongly affected by other mechanisms, such as phonon-assisted tunneling, impurity-assisted tunneling, and scattering. The voltage positions of the current density peaks and valleys are, however, easier to establish, since they are related to energy levels of the subbands.

The computed values of the current density strongly depend on the choice of the intrinsic device parameters. The most important parameters are the effective electron mass and the relaxation time. Thus, the choice of the intrinsic parameters is crucial for the accurate quantitative simulation of the resonant tunneling heterostructures. However, we expect the general tendencies observed here to be correct.


## 6  Conclusion

The system of fully discretized coupled nonlinear algebraic equations, which follows from (1), is possible to solve avoiding the use of decoupling algorithms, procedures, or methods. The results obtained for different resonant tunneling heterostructures using TQDDM show that the electron density is strongly nonlinear and asymmetric in both, QWs and barriers, under the influence of an external potential. However, in the equilibrium case ($U = 0$ V), perfect symmetry is present. The IV characteristics of the heterostructure nanodevices are quite different, when varying the thickness and the number of QWs of the device. In particular, changing the thickness of the QW, the peak and the valley current density change significantly, while the peak and the valley potential only slightly differ. In contrast, changing the number of the QWs (keeping the size of the QW constant), the peak and the valley potential change dramatically, while the peak and the valley current are almost unchanged.

# References

1. Sze, S.M.: Semiconductor Devices – Physics and Technology. Wiley, New York (1985)
2. Shur, M.: Physics of Semiconductor Devices. Prentice Hall, Englewood Cliffs (1990)
3. Yu, P.Y., Cardona, M.: Fundamentals of Semiconductors – Physics and Materials Properties. Springer-Verlag, Berlin Heidelberg New York (1996)
4. Scholl, E.: Nonlinear Spatio-Temporal Dynamics and Chaos in Semiconductors. Cambridge University Press, Cambridge (2001)
5. Ancona, M.G.: Diffusion-Drift Modeling of Strong Inversion Layers. COMPEL, 6 (1987) 11–18
6. Ancona, M.G., Tiersten, H.F.: Macroscopic Physics of the Silicon Inversion Layer. Phys. Rev. B, Vol. 35, No. 15 (1987) 7959–7965
7. Ancona, M.G., Iafrate, G.J.: Quantum Correction to the Equation of State of an Electron Gas in a Semiconductor. Phys. Rev. B, Vol. 39, No. 13 (1989) 9536–9540
8. Pinnau, R., Unterreiter, A.: The Stationary Current-Voltage Characteristics of the Quantum Drift-Diffusion Model. SIAM J. Numer. Anal., Vol. 37, No. 1 (1999) 211–245
9. Pinnau, R.: The Linearized Transient Quantum Drift-diffusion Model – Stability of Stationary States. ZAMM, 80(5) (2000) 327–344
10. Pinnau, R.: Numerical Approximation of the Transient Quantum Drift-Diffusion Model. Nonlinear Analysis, Vol. 47 (2001) 5849–5860
11. Pinnau, R.: A Note on Boundary Conditions for Quantum Hydrodynamic Equations. Appl. Math. Lett., 12 (1999) 77–82
12. Markowich, P.A., Ringhofer, C.A.: Stability of the Linearized Transient Semiconductor Device Equations. ZAMM, 67(7) (1987) 319–332
13. Markowich, P.A., Ringhofer, C.A., Schmeiser, C.: Semiconductor Equations. Springer-Verlag, Wien (1991)
14. Mock, M.S.: Analysis of Mathematical Models of Semiconductor Devices. Boole Press, Dublin (1983)
15. Selberherr, S.: Analysis and Simulation of Semiconductor Devices. Springer-Verlag, Wien New York (1984)
16. Schatzman, M.: Numerical Analysis – A Mathematical Introduction. Clarendon Press, Oxford (2002)

## Track on Computer Modeling and Simulation

## Track on Financial and Economical Modeling